JOURNAL OF GEOPHYSICAL RESEARCH, VOL. 104, NO. B1, PAGES 589-615, JANUARY 10, 1999

118.

Tsunami detection by satellite altimetry

Emile A. Okal

Department of Geological Sciences, Northwestern University, Evanston, Illinois

Alessio Piatanesi and Philippe Heinrich

Département Analyse et Surveillance de l'Environnement, Commissariat à l'Energie Atomique, Bruyères-le-Châtel, France

Abstract. We present what is to our knowledge the first direct observation of the deformation of the surface of the ocean upon passage of a tsunami wave, on the high seas, far from the influence of shorelines and continental shelves. We use satellite altimetry data from the ERS-1 and TOPEX/POSEIDON programs, complemented by spectrogram techniques and synthetic maregrams to examine the case of seven recent tsunamigenic earthquakes. We make a positive identification of the tsunami wave field in the case of the 1992 Nicaraguan tsunami, which we detect at 15°S, 106°W, five hours after origin time. We model the observed spectrogram by injecting a synthetic of variable amplitude into the signal of a repetitive cycle of the satellite along the same track, concluding that the Nicaraguan tsunami had a zero-to-peak amplitude of 8 cm in that region. In the case of the 1995 Chilean tsunami, a large scatter in the spectral properties of the reference tracks renders the detection tentative. We fail to detect the tsunamis of five other large events, including the 1996 Biak and 1996 Peru earthquakes, primarily on account of unfavorable source directivity in the geometry of existing satellite tracks, and of the strong and incoherent noise produced by large current systems, such as the Kuroshio in the Northwest Pacific.

1. Introduction and Background

While tsunamis are routinely recorded by tidal gauge stations located at continent or island shorelines, they have never, to our knowledge, been recorded directly on the high seas. This is due to the combination of relatively small wave amplitudes (estimated at less than 1 m even for exceptionally large events) and very large wavelengths ($\Lambda \geq 100$ km), which prevents any direct observation of the deformation of the surface of the ocean. The only reported detections involved ocean-bottom pressure gauges which recorded the Petatlan, Mexico tsunami of March 14, 1979 during a deployment at the mouth of the Gulf of California [*Filloux,* 1982], and similar devices later deployed in the Gulf of Alaska, which detected the tsunamis generated by the intraplate earthquakes of November 30, 1987 and March 6, 1988 [*González et al.,* 1991]. In contrast, records from ocean-bottom seismometers tethered to the shoreline [e.g., *Okada,* 1991; *Imamura and Shuto,* 1993] remain regional in character and do not sample the tsunami field at distances from the coast that are large compared to the wavelength.

This inability to document the amplitude of the tsunami wave on the high seas is unfortunate since the only measurable record of a tsunami then consists of tidal gauge amplitudes at coastal stations, which result from the complex, strongly nonlinear, effects accompanying the interaction of the wave with the coastal structure, on scales of hundreds of meters. In addition, these devices may have complex instrumental responses [*Braddock,* 1980]. Also, the generation of the wave occasionally involves poorly known parameters (such as the precise geometry of rupture) or structures (such as sedimentary layers). Thus it would be of great interest to obtain independent constraints in the form of the direct measurement of the amplitude of a tsunami wave on the high seas, since we would then be in a position to separate the generation of the tsunami (from earthquake source to high-seas amplitude) from its coastal interaction (from high-seas amplitude to run-up amplitude or tidal gauge record); as we stand now, we can study only the product of the two effects.

In the past few years, progress in satellite altimetry, in particular under the TOPEX/POSEIDON (T/P) project, has allowed the characterization of sea surface height variability [e.g., *Wunsch and Stammer,* 1995], the tracking of oceanic currents [*Teague et al.,* 1995], eddies [*Gründlingh,* 1995], Rossby waves [*Chelton and Schlax,* 1996], and the monitoring of the rise and fall of lakes and inland seas [*Birkett,* 1995; *Cazenave et al.,* 1997]. The amplitude of the altimetric signals for many of these phenomena is on the order of a few centimeters; their wavelengths are typically hundreds to thousands of kilometers, and their characteristic times range from weeks to years. Such observations then suggest that it might be possible, at least in principle, to detect a tsunami wave on the high seas by satellite altimetry. Indeed a number of attempts have been reported [e.g., *Callahan and Daffer,* 1994], but to our knowledge all have up to now been unsuccessful.

In this paper, we present a systematic search involving seven recent tsunamis. With the help of synthetic waveforms and spectrogram techniques, we make a positive identification in the case of the 1992 Nicaraguan tsunami, where the amplitude detected is 1.5 times that predicted by our synthetics, and a tentative one in the case of the 1995 Chilean tsunami. We dis-

Paper number 1998JB00018.
0148-0227/99/1998JB00018$09.00

Table 1. Earthquake and Satellite Data Used in This Study

Region	Event							T/P data		
	Date and Time		Epicenter		Depth,	Moment	Focal Geometry	Track	Target	Reference
	Date (DOY), Year	UT	°N	°E	km	10^{27} dyn-cm	ϕ, δ, λ		Cycle	Cycles
Nicaragua	Sep. 2 (246), 1992	0016:01.7	11.2	-87.8	15	3.4	122, 78, 90	523*, 525*	005	004,006
Java	June 2 (153), 1994	1817:36.8	-11.03	113.04	15	5.3	278, 7, 89	77	63	61-65
Japan Sea	July 12 (193), 1993	1317:11.9	42.71	139.28	16	4.7	179, 55, 90	127	30	28, 29, 32
Kuriles	Oct. 4 (277), 1994	1322:55.8	43.6	147.63	68	30	158, 41, 24	201	75	73-77
Chile	July 30 (211), 1995	0511:23.6	-23.34	-70.29	46	12.	354, 22, 87	230	105	103-107
Biak, Indonesia	Feb. 17 (048), 1996	0559:33.7	-0.63	136.59	15	22	114, 11, 91	73, 75	126	124-128
Chimbote, Peru	Feb. 21 (052), 1996	1251:04	-10.06	-80.17	15	2.16	153, 75, 88	180	126	122-132

DOY, (Julian) Day Of Year.
* ERS-1 data.

cuss probable reasons for our failure to detect the other tsunamis.

2. Data Set and Methodology

We concentrate here on seven tsunamigenic earthquakes spanning the years 1992–1996, whose principal parameters are listed in Table 1. These events and their respective tsunamis have been described by *Schindelé et al.* [1995], *Ruegg et al.* [1996], *Tanioka et al.* [1996], *Newman and Okal* [1996], and *Guibourg et al.* [1997]. Smaller tsunamis, such as the Halmahera event of January 21, 1994, or those taking place in small closed seas, such as the Flores Sea event of December 12, 1992, are not included.

The satellite altimetry data sets used in this study consist of T/P corrected sea surface heights. In the case of the 1992 Nicaraguan earthquake, which occurred during the verification phase of the T/P project, we use ERS-1 data.

We seek to detect the tsunami signal where it is expected to be largest, i.e., when the satellite track would cross the initial wavefront, hopefully at a steep azimuthal angle, and in the first few hours following its generation, before geometrical spreading on the spherical Earth and dispersive propagation significantly reduce the amplitude of the wave. Potential hits were identified by comparing the ephemerides of individual satellite tracks with digital travel-time maps computed using a smoothed ocean bathymetry and the algorithm of *Woods and Okal* [1987]. Example of suitable tracks are given on Figure 1.

For each track so identified, we isolated in the sea-surface-height signal a segment of time series varying from 549 to 1367 s in duration (or 3856 to 7931 km in sea surface track), which we call the "target" data series. In the case of the 1993 Japan Sea tsunami, the data series are much shorter since they are limited to that inland sea. We also extracted similar series for repetitive cycles along the same track, which we call "reference" data series. The latter can be regarded as the background noise out of which we seek to extract a signal. The repeat periods of the satellites (35 days for the multidisciplinary phase of ERS-1; 9.916 days for T/P) should allow the elimination of any seasonal effect (and of static components expressing the short-wavelength geoid) in the differential series obtained by subtracting any reference series from the target series.

The altimetry profiles shown in this study are oriented mostly North-South. Some are ascending tracks, i.e., with time increasing Northwards, and others descending. For a uniform presentation of the data, descending series were reversed and all profiles will be presented with latitude increasing from South to North along the profile.

2.1. Spectral Analysis

Ideally, and for a sufficiently large deformation of the ocean surface, one could hope to detect a decimetric tsunami signal by direct visual inspection of the unprocessed target series, or possibly of the differential series. However, in all cases involved (with the marginal exception of Track 525 of the 1992 Nicaraguan tsunami), no such signal prevailed over background noise. For this reason, we proceeded to Fourier-transform the data series and analyze their spectra.

The data series consist of measurements taken at regular time intervals aboard the satellite (occasionally corrected by linear interpolation when a few points were missing). Since the latter orbits at a ground velocity of approximately 6–7 km/s, each point in the series is displaced from the previous one both in time ($\delta t = 0.98$ s (ERS-1); 1.17 s (T/P)) and space on the ocean surface ($\delta d = 7.06$ km (ERS-1); 6.77 km (T/P)). Because of the large disparity in surface velocity between the spacecraft (7.2 km/s (ERS-1); 5.8 km/s (T/P)) and the expected tsunami wave (typically 210 m/s for an ocean depth of 4500 m), any data series represents more a snapshot of the surface of the ocean at a given time than a maregram at a given point, and it approaches more a "space series" than a "time series". Accordingly, the "frequency" in the Fourier space resulting from the application of a standard transform to the data series is hybrid in nature but approaches a spatial frequency sampling the wavenumber space, which we will conveniently characterize with units of inverse distance (km^{-1}). Spectral amplitudes will then have units of squared length (m^2). Note however that the resulting "wavenumbers" k_t are measured along the satellite track, which is generally oriented at an angle to the local tsunami ray, and thus may not be representative of the true wavenumbers k of the tsunami field at the corresponding space-time combination.

We further use the standard spectrogram technique, originally introduced in geophysics by *Landisman et al.* [1969], and consisting of Fourier-transforming a moving window in the original data set. This identifies the exact portion(s) of the data series contributing energy at a given k_t, in particular in relation to the causality of any window with respect to the expected timing of the tsunami wave field. For all spectrograms shown in this study, the length of the moving windows was 2^6 points (or 452 km for ERS-1 and 433 km for T/P), and the interval between windows was 7 samples (or 49.4 km for ERS-1 and 47.4 km for T/P). The spectrograms were then interpolated and plotted using 50–km pixels.

2.2. Tsunami Synthetics.

We generate synthetic profiles ("synthetics") of tsunami amplitudes expected along the various tracks in the following

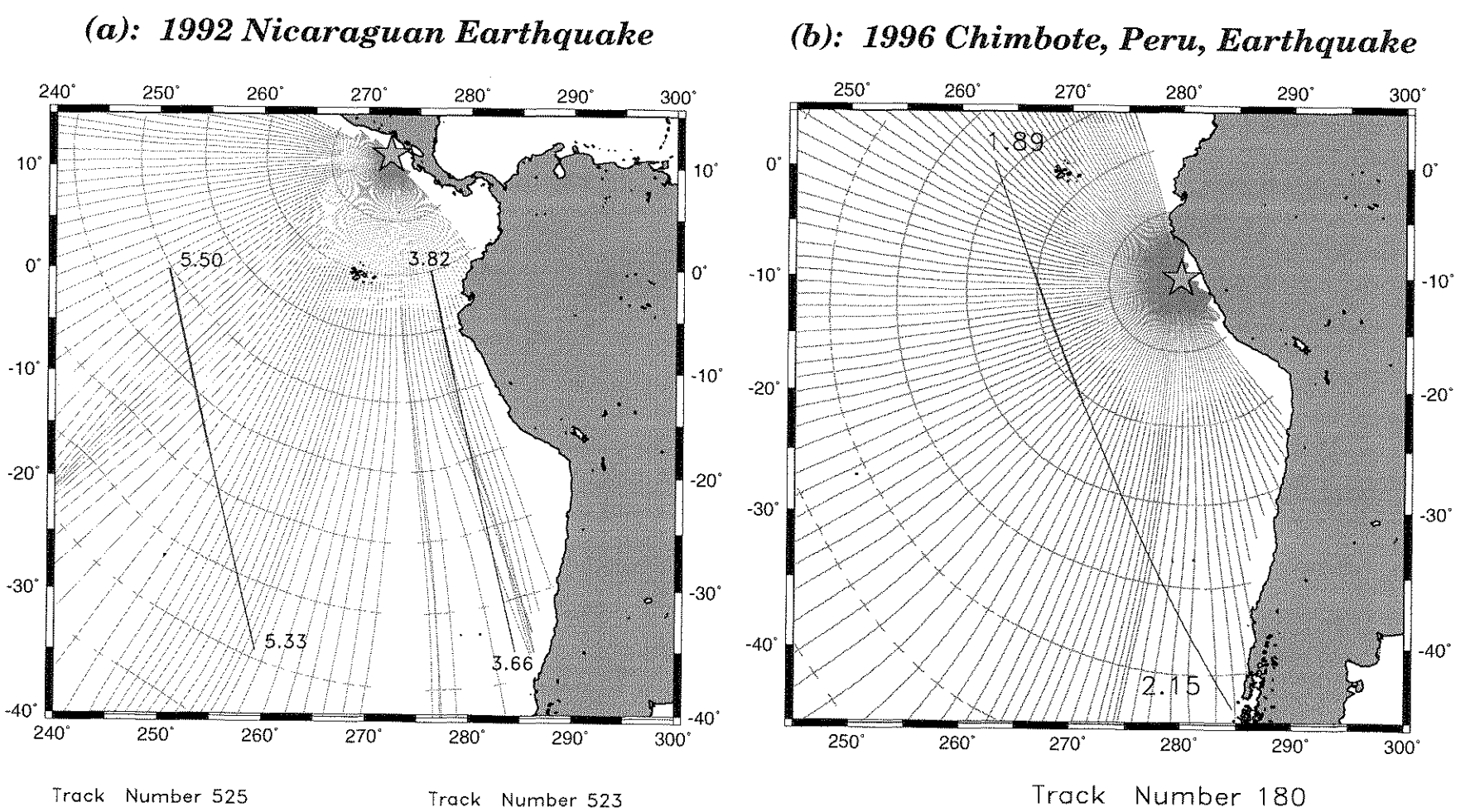

Figure 1. (a) Map of satellite tracks used for the 1992 Nicaraguan tsunami. The half-tone lines are rays traced from the epicenter (star) leaving at intervals of 2° in azimuth and stopped at the coastlines [*Woods and Okal,* 1987]. Tick marks delineate the progress of the wave front in hours after the origin time of the centroid solution (0016:42 UT). The two segments are the trajectories of Tracks 523 and 525 of ERS-1 Cycle 005, between 40°S and 0°S, with the numbers showing the time (in decimal hours) elapsed since origin time at the beginning and end of each track segment. The thicker traces identify those portions inside the wave field, where signals are expected to be causal. (b) Same as Figure 1a for the 1996 Chimbote tsunami. The only available trajectory is Track 180 of T/P Cycle 126. The origin time of the event is 1251:04 UT.

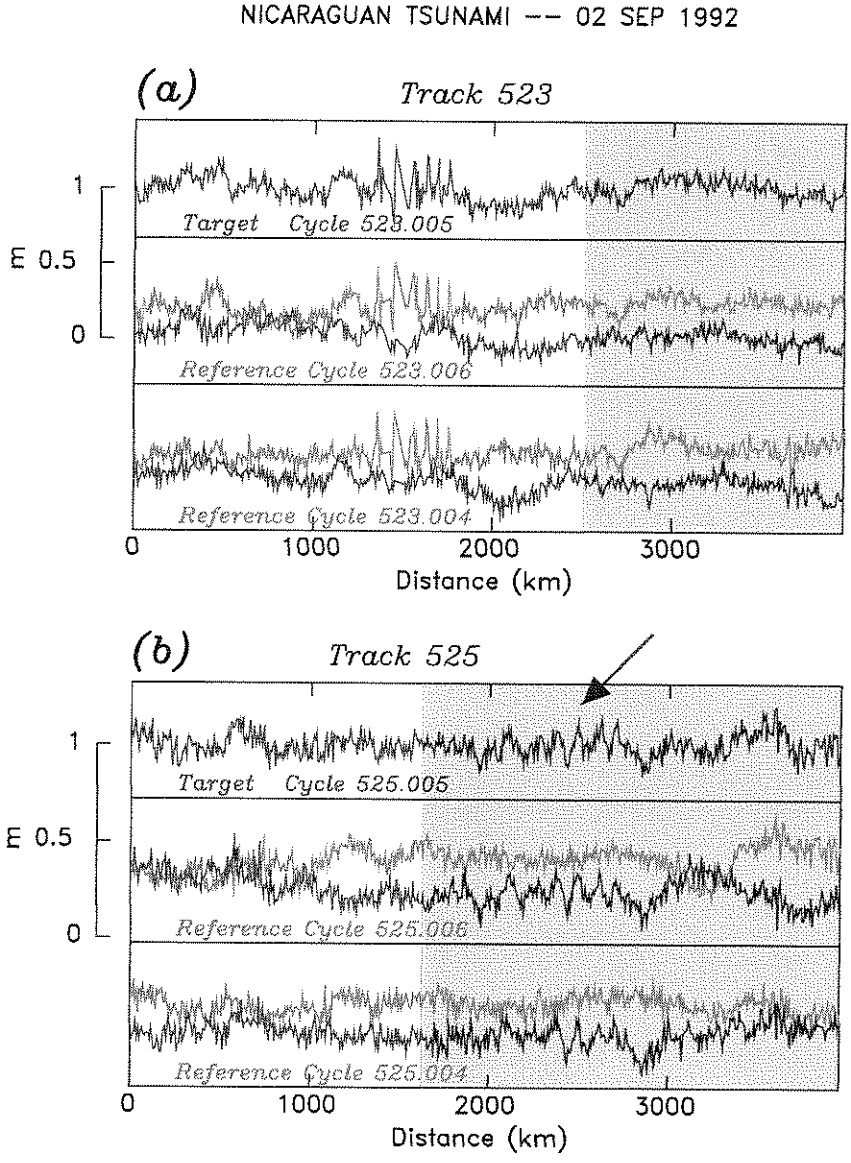

Figure 2. ERS-1 Data series for the 1992 Nicaraguan tsunami: (a) Track 523 and (b) Track 525. In both cases, the top frame shows the target series from Cycle 005, where the tsunami signal is expected. Abscissa is distance along track, starting in the South. In the other frames, the top trace is the reference series for another cycle along the exact same track; the bottom trace is the difference between the target and reference series. The vertical scale is common to all plots for the same track. The shaded bands indicate the portion of the tracks located inside the wave field, where signals are expected to be causal. In Figure 2a, note that the strong signal, ~1600 km into the series, and present in all three cycles, is related to the geoid. In Figure 2b, the arrow identifies the signature of the tsunami signal, as inferred from Plate 1.

way. Starting with a model of the static ocean-bottom displacement derived from the earthquake's moment tensor [*Okada,* 1985], we use a finite difference code [*Mader,* 1988; *Guibourg et al.,* 1997] to create a full three-dimensional space-time grid of the expected wave amplitude, which we then interpolate to recreate a synthetic series with the exact same time and space sampling as the target altimeter data series.

Such synthetics could be inaccurate for several reasons. First, even though the moment of the earthquake is usually well constrained, and the fault length L can be estimated from directivity studies [*Ben-Menahem,* 1961], the traditional trade-off subsists between amplitude of slip, D, and area of rupture $S = L\,W$. Although normal mode theory predicts that the overall amplitude of the tsunami wave at teleseismic distances should be controlled only by the moment tensor of the source [*Ward,* 1980; *Okal,* 1982], its spectral content could be affected by the details of the rupture geometry. Additionally, the involvement of sedimentary structures in the hypocentral area could significantly affect both the spectral content of the wave and its overall amplitude [*Okal,* 1988]. It is in this very general framework that we take our synthetics as representative of the expected signal that we seek in the target data series.

2.3. Injecting the Synthetic into a Reference Signal

In order to determine the feasibility of extracting a signal (represented by our synthetic series) from the background noise

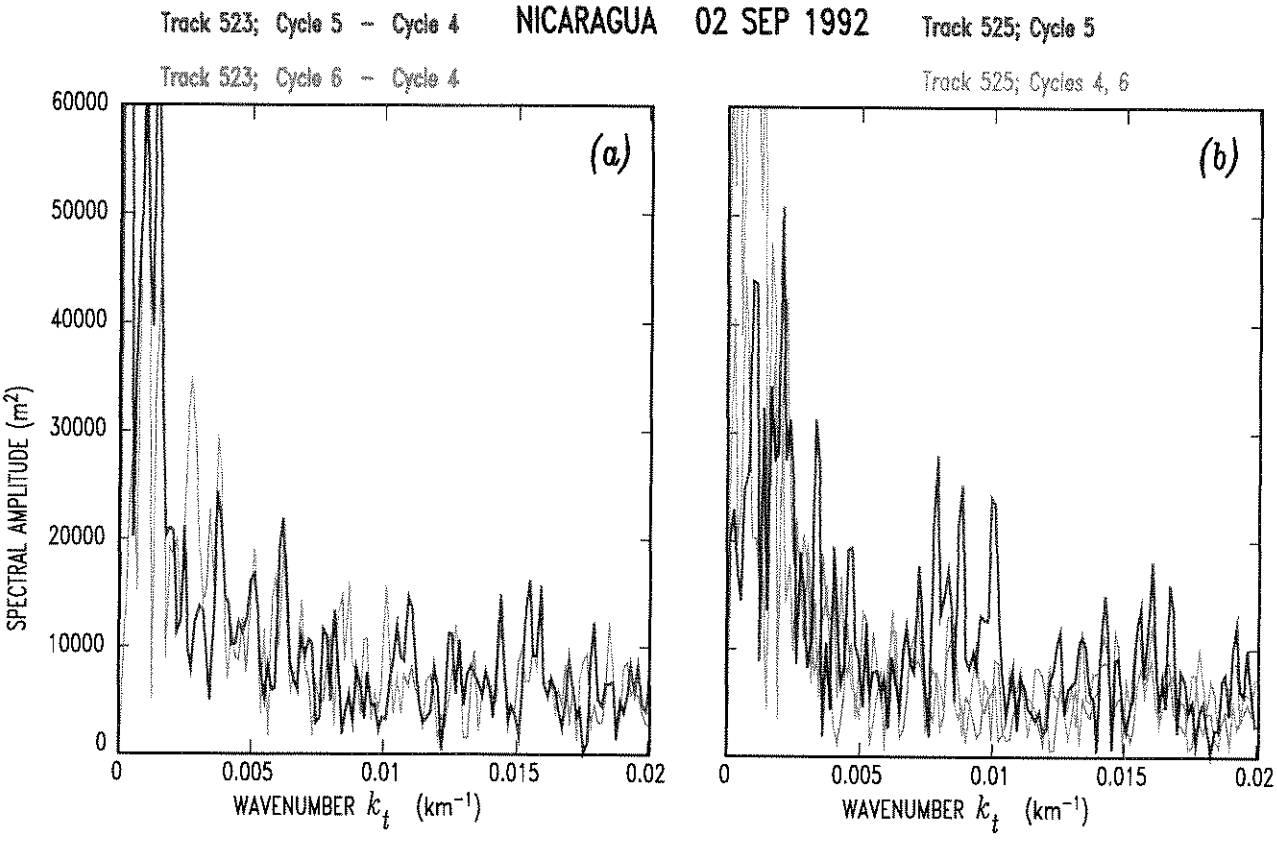

Figure 3. Spectral amplitude of the target series (thick trace) and reference series (thin traces) for the 1992 Nicaraguan tsunami. (a) Track 523. In this instance, the data processed consist of the difference between Cycles 5 and 4 (target series) and between Cycles 6 and 4 (reference series). Note the absence of signal in the target series. (b) Track 525. Note the significant spectral amplitude at 0.007–0.01 km^{-1}.

(represented by the reference series), we conducted the following experiment: we added the synthetic series (multiplied by a variable amplitude factor α) to a reference series for the same track, and analyzed the spectrogram of the resulting series. We varied both the reference cycle (to illustrate the variable level of noise depending on climatic conditions) and the value of α, which ranged between 0.1 and 100. Only a sample of the spectrograms computed will be shown.

This technique can achieve either of two goals: upon positive identification of a tsunami signal, the spectral amplitudes of the target spectrogram can be used to best-fit α, thus providing a measurement of the amplitude of the detected tsunami on the high seas; if on the other hand, we fail to detect the tsunami signal, we can similarly infer a maximum amplitude for its wave.

3. The 1992 Nicaraguan Tsunami: Positive Detection

We recall that this event qualified as a "tsunami earthquake", i.e., that its tsunami was larger than expected from its seismic waves [*Kanamori,* 1972], due to an exceptionally slow rupture [*Kanamori and Kikuchi,* 1993; *Newman and Okal,* 1998].

We use altimetry data from Tracks 523 and 525, Cycle 005 of the ERS-1 mission (Figure 1), with Cycles 004 and 006 as references series. Both tracks are ascending, traveling from South to North, approximately 3.7 and 5.4 hours after the event, respectively. They are expected to penetrate the tsunami wave field around 11°S and 17°S respectively. The corresponding signals are shown on Figure 2, and their spectra on Figure 3.

For Track 523, all cycles are dominated by strong permanent signals reflecting geoid anomalies, in particular in the vicinity of the Nazca Ridge (19°S or 1600 km into the series). For this reason, we take as our target series the difference between Cycles 005 and 004, and as reference series, the difference between Cycles 006 and 004. As shown on Figure 3, the former rises only marginally above the noise level defined by the latter, and we must conclude that no signal can be extracted from the space series of Track 523.

On the other hand, in the case of Track 525, which misses the Nazca Ridge and its accompanying perturbations in the geoid, we find it unnecessary to compute differences between tracks, and instead use the raw track data as target and reference series. Figure 3b shows that Track 525, Cycle 005 exhibits significant spectral amplitudes ($\approx$ 25,000 m^2) in the band 0.007–0.01 km^{-1}, about twice the amplitude of the corresponding spectra for the reference cycles. Spectrograms for Track 525 are shown on Plate 1. For the target cycle, Plate 1a indicates that the large spectral amplitudes are confined to the wavenumber range $k_t \leq 0.015$ km^{-1}, in the distance window 2000–2800 km from the beginning of the trace, or from latitudes 17°S to 10°S, i.e., at the expected location of the tsunami wave front. While some energy is present in the noncausal part of the target series (400 to 1300 km into the series), both its amplitude and spectral characteristics are comparable to

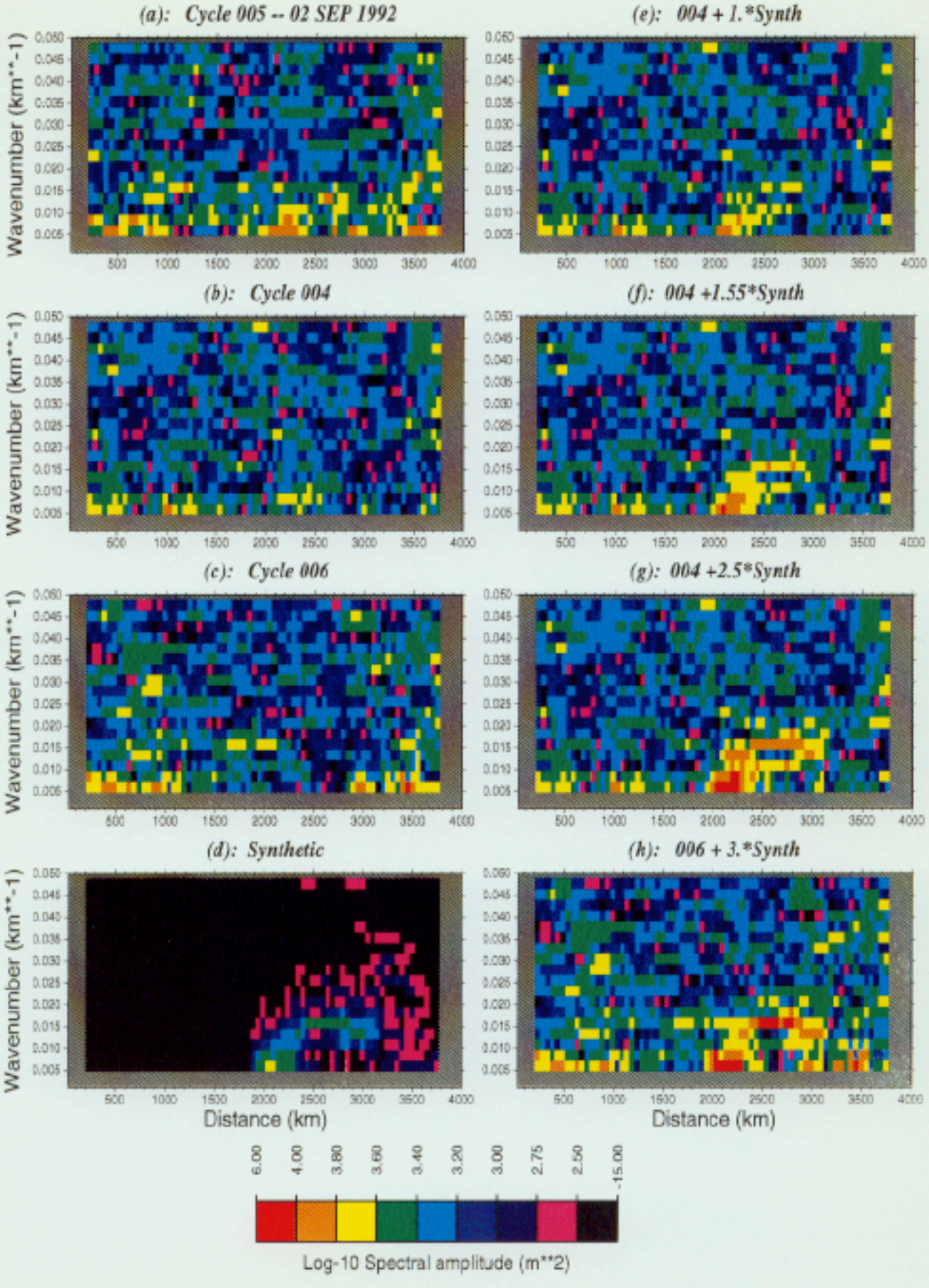
(a): Cycle 005 -- 02 SEP 1992
(b): Cycle 004
(c): Cycle 006
(d): Synthetic
(e): 004 + 1.*Synth
(f): 004 +1.55*Synth
(g): 004 +2.5*Synth
(h): 006 + 3.*Synth
Wavenumber (km**-1)
Distance (km)
6.00
4.00
3.80
3.60
3.40
3.20
3.00
2.75
2.50
-15.00
Log-10 Spectral amplitude (m**2)

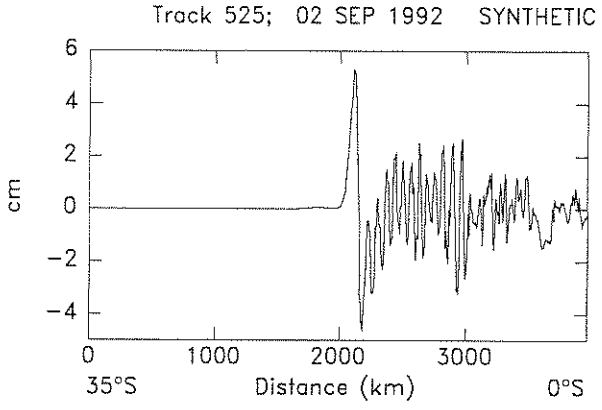

Figure 4. Synthetic maregram computed along Track 525 for the 1992 Nicaraguan tsunami.

those of reference Cycle 006 in the same distance window (Plate 1c). The latter is also significantly noisy at very low wavenumbers at the northern end of the track. By contrast, Reference Cycle 004 (Plate 1b) is much quieter throughout the distance-wavenumber plane.

It is interesting to note that the spectrum of the target cycle between distances of 2000 and 2700 km into the series exhibits some level of "spatial dispersion": the low wavenumbers (0.005 km^{-1}) are sampled at 2050–2400 km, while the higher wavenumbers (0.012 km^{-1}) are sampled around 2750 km, i.e., farther North along the track, or closer to the epicenter. This systematic pattern is absent from the spectrogram of the reference series.

A synthetic maregram was computed for Track 525 using *Piatanesi et al.*'s [1996] source deformation model, and is presented in Figure 4 (space series) and Plate 1d (spectrogram). The latter exhibits a spatial dispersion remarkably similar to that described above: the lower wavenumbers (0.005 km^{-1}) are present between 2000 and 2300 km, and the higher ones (0.015 km^{-1}) between 2500 and 3000 km. The corresponding difference in epicentral distance is 9%, but a direct interpretation of this observed dispersion in terms of the true dispersion of the tsunami wave field is made difficult by the fact that our wavenumbers k_t are measured along track, at an angle θ close to 45° from the tsunami rays, and are thus $\cos\theta = 0.7$ times the true wavenumbers k of the tsunami wave field, the relevant periods sampled being 850 and 350 s, respectively. The suggested 9% dispersion between those periods is slightly larger than the 7.7% measured by *González and Kulikov* [1993] on the ocean-bottom signals from the 1988 Gulf of Alaska earthquake; the difference is however easily explained by the fact that our paths sample shallower seas, where dispersion is expected to be stronger at comparable wavenumbers.

Injection experiments were performed using both Reference Cycles 004 and 006 as noise. In general, the former gave spectrograms more in line with that of the target series; Plates 1e, 1f, and 1g show corresponding spectrograms for $\alpha = 1$, 1.55, and 2.5, respectively. The central value is the estimate optimizing the general pattern of computed and observed spectrograms. The target series, however, retain a significant noise level in their noncausal segment, which would be better modeled by injecting the synthetic into Reference Cycle 006, as documented by the spectrogram in Plate 1h.

The conclusion from Plate 1 is a good correlation between the distance-wavenumber combination of the pulse of energy observed in the target series and that predicted by the synthetic: the pulse is found at the right place at the right time, it has the right wavenumber, and it exhibits the predicted dispersion. On the basis of this evidence, and especially of the latter observation, we propose that the signal detected in the spectrogram of Track 525, Cycle 005 between distances of 2000 and 2800 km is the tsunami wave field of the Nicaraguan earthquake. Note that matching the energy levels of the target series and the synthetic would require a tsunami 1.55 times larger than synthesized, corresponding to a zero-to-peak amplitude of 8 cm, which is also in general agreement with the oscillations identifiable in that distance window in the space series (see arrow on Figure 2b).

Finally, the difference in results between Tracks 523 and 525 (no signal along the former despite a wavefront crossing earlier after the origin time) is easily explained by source directivity. Following *Ben-Menahem* [1961], we compute the directivity coefficient $D(\phi)$ for a surface wave observed in the far field at the azimuth ϕ from a fault of length L rupturing at velocity V_R as

$$D(\phi) = \frac{\sin Y}{Y} \qquad \text{with} \qquad Y = \frac{k\,L}{2}\left[\frac{c}{V_R} - \cos\phi\right] \tag{1}$$

where k is the wavenumber of the tsunami and c its phase velocity. For hypersonic rupture velocities ($V_R/c \gg 1$), it is a classical result that D is maximum at right angles from the direction of rupture [*Ben-Menahem and Rosenman,* 1972; *Okal and Talandier,* 1991]. Using published values of the geometry and rupture velocity of the Nicaraguan event [*Kikuchi and Kanamori,* 1995], we find $\phi = 70°$ and $D = 61\%$ for Track 525, but $\phi = 28°$, and only $D = 17\%$ for Track 523. This more than compensates for the amplitude effects of geometrical spreading and dispersion along the different lengths of the two tracks. This is confirmed by the maximum amplitudes of the synthetics computed for the two tracks: 9.8 cm peak-to-peak for Track 525 versus only 4.3 cm for Track 523. This remark illustrates the crucial influence of directivity on tsunami amplitudes; in this respect, it is interesting to note, following *Okal and Talandier* [1991], that directivity lobes for tsunamis are narrower than for conventional seismic waves, further hampering the potential detection of tsunami signals by satellite altimetry.

Plate 1. Spectrograms for the Nicaraguan tsunami along Track 525. Distance is along track from the southern end of the series. (a) Target series. This frame shows that the energy identified at 0.015 km^{-1} on Figure 3 is concentrated around a location 1600-2000 km into the series, and as such, noncausal with respect to the tsunami source. (b, c) Same as Plate 1a for Reference Cycles 004 and 006. (d) Same as Plate 1a for the synthetic maregram. The black bands define the extent of the noncausal segment in the target series. Plates 1e ($\alpha = 1$), 1f ($\alpha = 1.55$), and 1g ($\alpha = 2.5$) are the same as Plate 1b after a fraction α of the synthetic maregram is injected into the reference series for Cycle 004. Note that the energy of the tsunami signal becomes comparable to that in the causal segment of the target series (Plate 1a) for $\alpha = 1.55$ (Plate 1f), suggesting detection of a tsunami with zero-to-peak amplitude 8 cm. (h) Same as Plate 1e, using Cycle 006 as reference, and $\alpha = 3$.

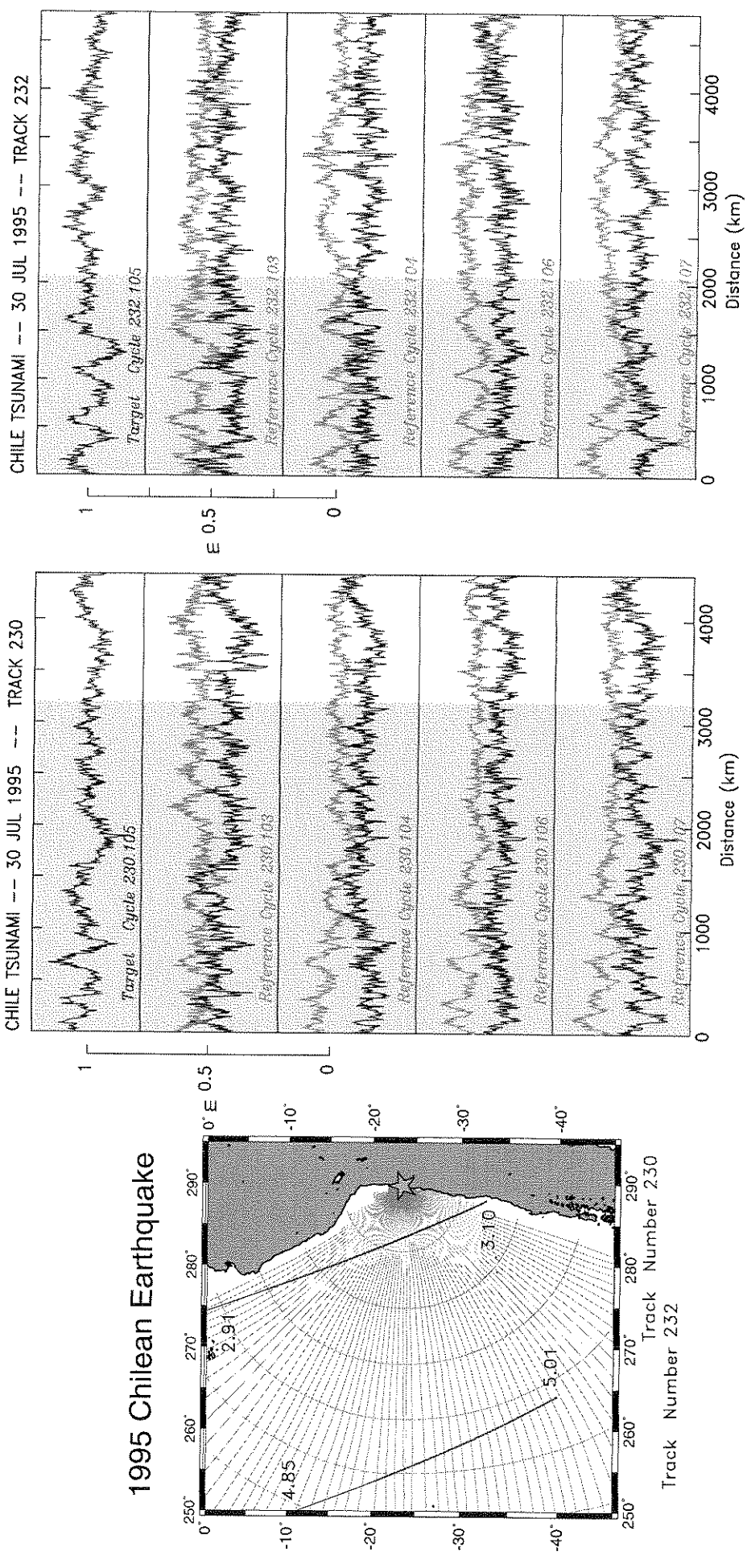

Figure 5. Map and plots of target and reference series for the 1995 Chilean tsunami. (left) Map (similar to Figure 1); (center) Track 230; (right) Track 232 (both similar to Figure 2).

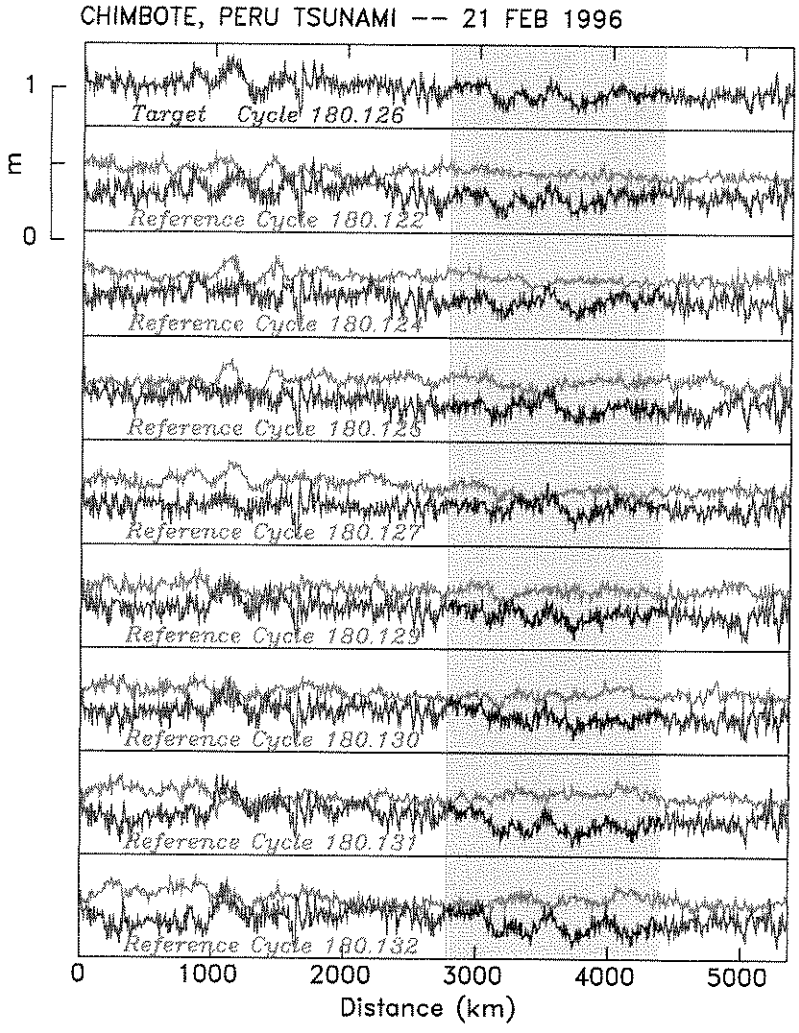

Figure 6. Same as Figure 2 for the 1996 Chimbote, Peru earthquake.

4. The 1995 Antofagasta, Chile Tsunami: Tentative Identification

This relatively large earthquake ($M_0 = 1.2 \times 10^{28}$ dyn-cm) generated a powerful tsunami, which ran up 2 m in the Marquesas Islands, where it sank a boat in a harbor, 7500 km away from the epicenter. Two profiles are available during T/P Cycle 105: Track 230 sampling the wave field 3 hours after origin time, and Track 232 farther out at sea, 5 hours after origin time (Figure 5).

Synthetics computed for the rupture model of *Guibourg et al.* [1997] suggest an amplitude of 10 cm peak-to-peak along Track 230, with the energy concentrated mostly at 0.007 km^{-1}, approximately 1500 km into the series. The spectrogram of Cycle 105 does not match these characteristics, being dominated by energy at lower wavenumbers, and remarkably quiet in the central part of the expected wave field. We conclude that no signal is detected in Track 230. This is probably due to the fact that the section of track intersecting the wave front (its northernmost part) suffers from unfavorable source directivity.

Spectrograms for Track 232 are presented in Plate 2. Synthetics suggest an amplitude of 11 cm peak-to-peak with energy concentrated in two peaks, one 500 km into the series, at 36°S, and the other, stronger one 1700 km into the series, at 25°S, closer to the point where the profile leaves the causal wave field. Wavenumbers are generally low, in the range 0.003 to 0.005 km^{-1}. Examination of the spectrogram of the target profile (Cycle 105) indeed reveals remarkably low amplitudes in its noncausal parts, with a strong burst of energy at 0.003 to 0.006 km^{-1} between 1500 and 1850 km into the series, and sustained energy at 0.003 km^{-1} between 450 and 1100 km. The former signal is absent from most reference cycles, with Cycle 104, however, being relatively noisy. Injection experiments suggest that the northern section of the wave field (from 1500 to 1900 km into the series) is well modeled by superimposing 1.5 times the synthetic onto Cycle 107, considered as "noise", but also possibly by using a lesser synthetic amplitude (0.7) and the noisier reference cycle 104. Given the uncertainty on the amplitude of the synthetic to be injected in order to match the observed spectrogram, we regard the detection of the tsunami signal as tentative.

5. The 1996 Chimbote, Peru, Tsunami: Failure to Detect

With $M_0 = 2 \times 10^{27}$ dyn-cm, this "tsunami earthquake" was only slightly weaker than the Nicaraguan event, and generated a damaging tsunami on the Peruvian coast [*Tanioka et al.*,

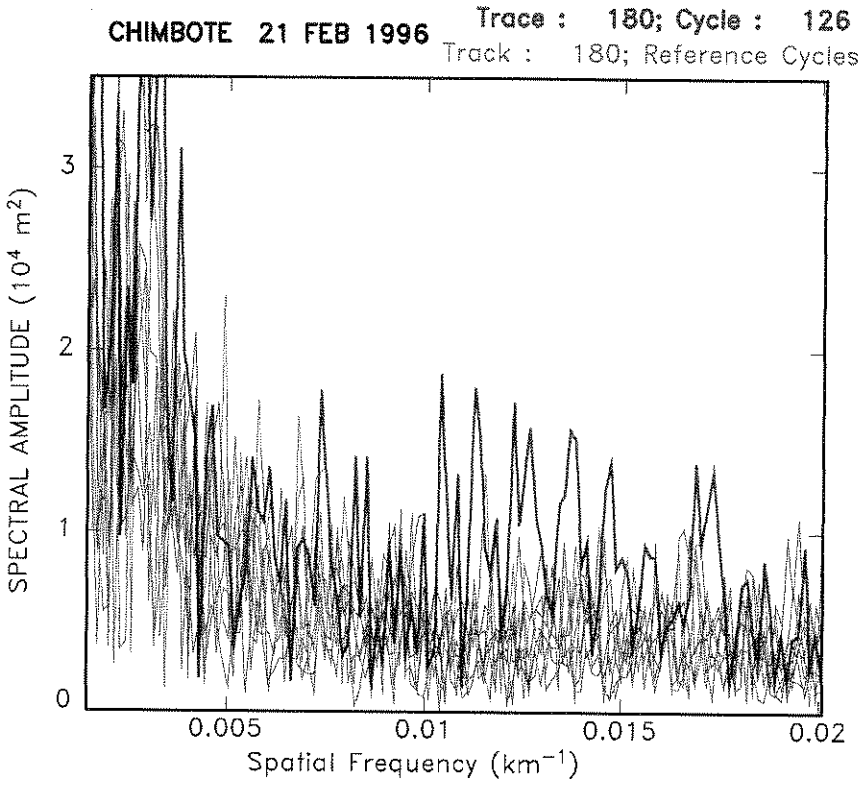

Figure 7. Spectral amplitude of the target series (thick trace) and reference series (thin traces) for the 1996 Chimbote tsunami. Note that the target spectrum has significant energy in the 0.01–0.015 km^{-1} range. The experiment in Plate 3 shows that this signal is, however, non causal.

1996]. A promising altimetric signal turned out to be unrelated to the tsunami.

The tsunami signal is expected on Track 180 of T/P Cycle 126, with reference series from Cycles 122, 124, 125, 127, 129–132. The track is descending and was reversed. As shown on Figure 6, neither direct visual inspection of the target series, nor the subtraction from it of a reference series, results in obvious detection of a tsunami signal in the space domain.

Figure 7 shows the spectrum of the target data series, and compares it with those of the eight reference cycles. Only the target cycle, 126, exhibits a significant rise above noise level in the wavenumber range $k_t = 0.01$ to 0.015 km^{-1}. While the corresponding wavelengths (70 to 100 km) are shorter than would be expected for a tsunami wave, the possibility that the tsunami had significant short-period energy cannot be dismissed a priori. The spectral amplitude of the possible signal reaches 17,000 to 20,000 m^2.

Spectrograms are shown in Plate 3, comparable to Plate 1. Plate 3a confirms the absence of any detectable signal above noise level and, in particular, indicates that the peak at 0.015 km^{-1} in Cycle 126 takes place 1800 km into the target series, around 30°S, or 1100 km ahead of the tsunami wavefront. This spectral signal is therefore noncausal with respect to the tsunami source and cannot be associated with it, even though the signal was present only in the target series and absent from the reference series. This transient perturbation, whose origin is unknown, is present fortuitously on the day of the tsunami, and its spectrogram analysis underscores the care which must be taken before any association with the tsunami source can be proposed.

The synthetic series for Track 180 is shown on Figure 8. It exhibits two positive peaks of approximately +6 cm amplitude, and a trough of -6 cm amplitude, corresponding to the satellite entering the wave field in the South around 19°S (first peak), crossing the distorted ocean above the wave field, and then exiting the wave field in the North around 12°S (second peak). The spectrogram of the synthetic (Plate 3c) shows most of the energy concentrated in the center of the wave field, at wavenumbers $k_t \leq 0.010$ km^{-1} and with spectral amplitudes reaching about 10,000 m^2. We conclude that the spectrogram of the target trace on Plate 3a does not match the characteristics expected from the synthetic trace.

Plates 3d, 3e, 3f show results from the injection experiments, using Cycle 132 as reference signal, and $\alpha = 1$, 3, and 10, respectively. The expected amplitude of the tsunami, as modeled by the synthetic ($\alpha = 1$), remains too small to emerge

Plate 2. Same as Plate 1 for the 1995 Antofagasta, Chile tsunami. Shown are spectrograms for (a) the target cycle, (b, c) selected reference cycles (note higher level of noise in Cycle 104), (d) the synthetic maregram, and (e, f, g, h) injection experiments. Note that the target spectrogram is well modeled by injecting 1.5 times the synthetic into Cycle 107 (Plate 2f), but that a good fit would also be obtained with 0.7 times the synthetic superimposed on Cycle 104 (Plate 2h).

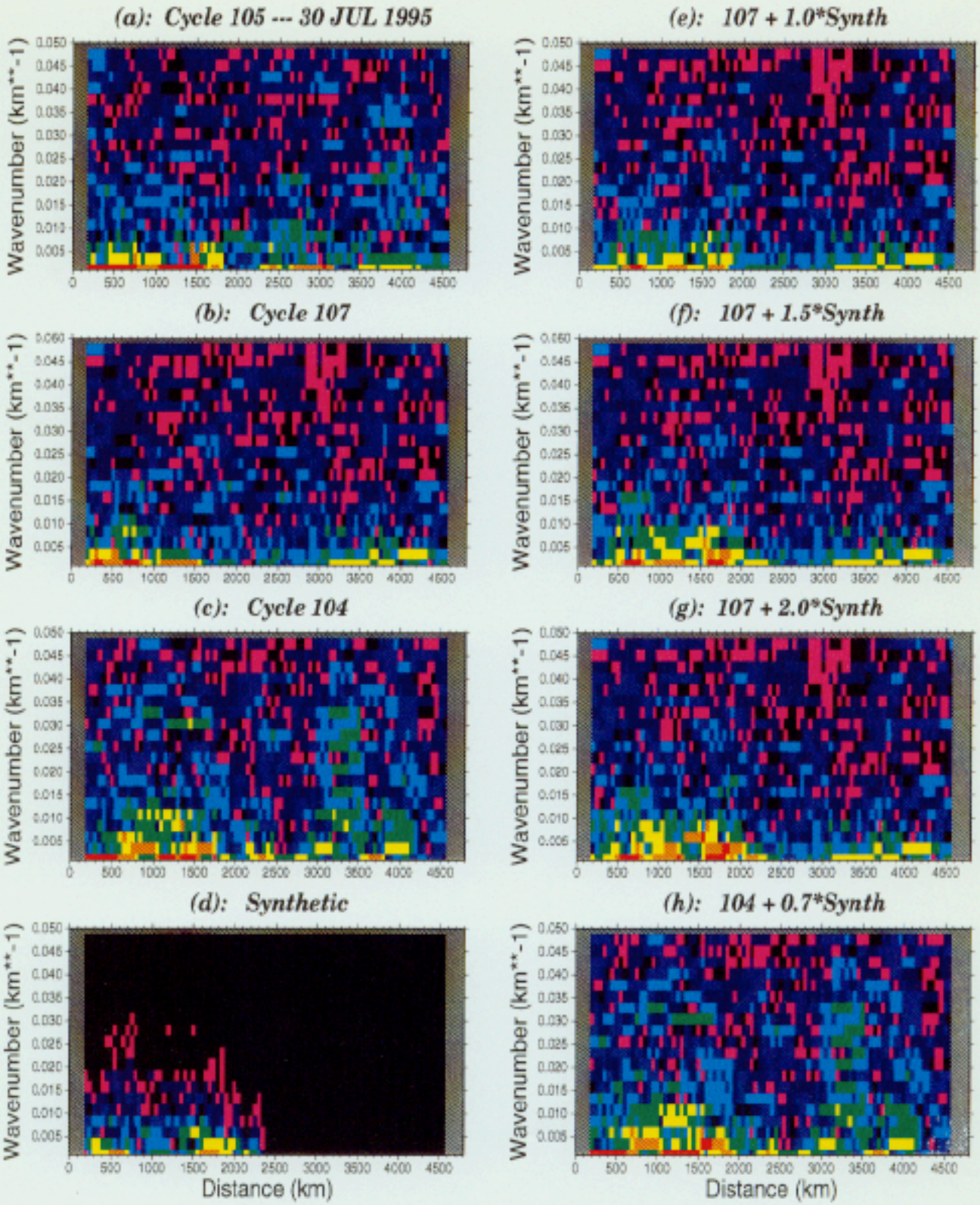
(a): Cycle 105 --- 30 JUL 1995
(b): Cycle 107
(c): Cycle 104
(d): Synthetic
(e): 107 + 1.0*Synth
(f): 107 + 1.5*Synth
(g): 107 + 2.0*Synth
(h): 104 + 0.7*Synth
Wavenumber (km**-1)
Distance (km)
6.00
4.00
3.80
3.60
3.40
3.20
3.00
2.75
2.50
-15.00
Log-10 Spectral amplitude (m**2)

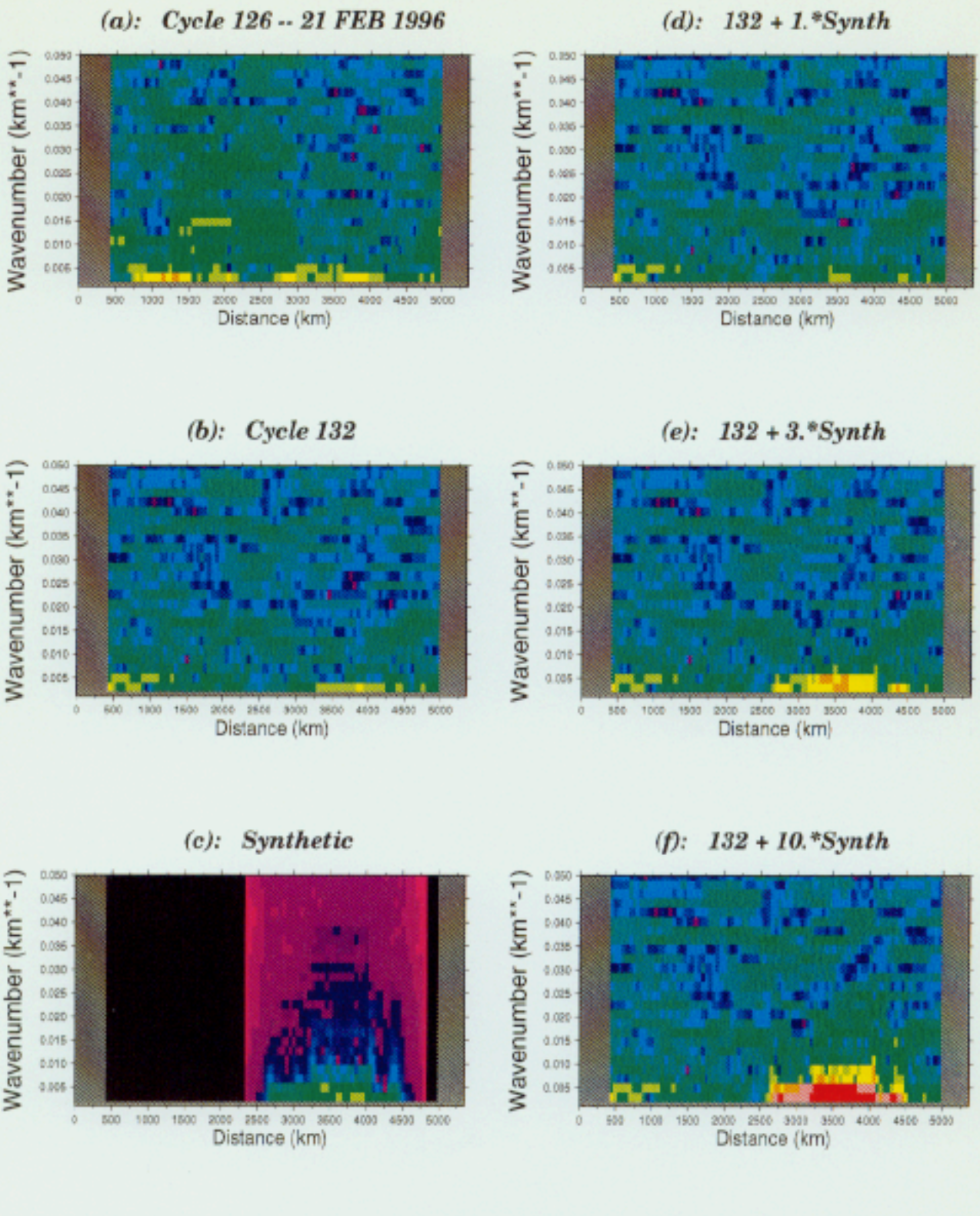
(a): Cycle 126 -- 21 FEB 1996
(d): 132 + 1.*Synth
(b): Cycle 132
(e): 132 + 3.*Synth
(c): Synthetic
(f): 132 + 10.*Synth
Wavenumber (km**-1)
Distance (km)
6.00
4.75
4.50
4.30
4.10
3.90
3.70
3.50
3.30
3.10
2.90
2.70
2.50
2.30
2.10
1.90
0.60
-0.70
-2.00
-10.00
Log-10 Spectral amplitude (m**2)

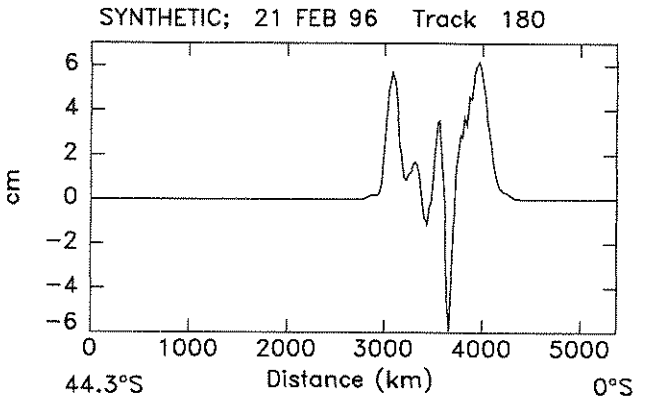

Figure 8. Synthetic maregram computed along Track 180 for the Chimbote, Peru tsunami of February 21, 1996.

from the noise, defined from the reference tracks as being typically 12,000 m^2 at the relevant wavenumber of 0.003 km^{-1}. Cycle 126 does show a slightly higher level of spectral amplitude at the latitudes expected for the tsunami wavefront, which could be interpreted as due to a tsunami with 1.5 to 2 times the amplitude of the synthetic. However, the presence of the noncausal energy in the southern part of the target series (both around 0.003 km^{-1}, 1300 km into the record, and at 0.015 km^{-1}, 1800 km into the record) renders this interpretation unwarranted: we cannot positively identify the tsunami in the target series of Cycle 126, and it would take a tsunami 2.5 to 3 times larger than synthesized (corresponding to amplitudes of 15–20 cm zero-to-peak, or spectral amplitudes of 16,000 m^2) to convincingly emerge from the noise (Plate 3e). This failure to detect the Chimbote tsunami is due to generally higher noise levels (as present in the reference series), rather than a demonstrably smaller tsunami.

6. Other Events

In this section, we discuss the case of the other tsunamis in Table 1, for which we failed to detect an altimetric signal.

6.1. The Biak Tsunami of February 17, 1996

With $M_0 = 2.4 \times 10^{28}$ dyn-cm, and at the time of writing (Oct. 24, 1998), this earthquake is the largest shallow interplate thrust event since the inception of the Centroid Moment Tensor catalog (*Dziewonski et al.,* [1983] and subsequent quarterly updates). It occurred along a segment of the New Guinea trench where no previous seismicity had been documented [*Okal,* 1996]. The associated tsunami was devastating on Biak and neighboring islands, where it reached run-up heights of 7 m; the toll from the combination of the earthquake and tsunami was upward of 100 fatalities. As such, this event was a promising candidate in our study, and our failure to detect a tsunami signal from space deserves some discussion.

Two ascending satellite tracks from T/P Cycle 126 are available immediately following the Biak earthquake (Figure 9): Track 073 crosses the tsunami wave field over the Ontong-Java Plateau to the East; it intersects the wavefront and becomes noncausal over the Marshall Islands, approximately 4.5 hours after origin time. Its orientation is expected to be unfavorable in terms of source directivity, but on the other hand, our ray-tracing experiments suggest focusing over the Caroline Sea and onto the Ontong-Java Plateau; additionally, the shallow depths over the plateau may result in higher surface amplitudes for the wave. Track 075 crosses the tsunami wave field over the West Mariana Basin of the Philippine Sea, the Bonin Islands, and the Northwest Pacific Basin, where it intersects the wavefront approximately 6.6 hours after origin time. This latter track would appear to have a better chance of sampling the tsunami field in the direction of maximum directivity at the source. However, it comes later (6 hours after the event), samples a region significantly disturbed by the Bonin-Marianas island arc, and in its northern part, close to the wavefront, enters a region of very high sea-surface variability [*Wunsch and Stammer,* 1995]. This area is traversed by the Kuroshio current, whose strong signal is expressed consistently (but not coherently between cycles) both in the target series and in the reference tracks (Figure 9), and effectively prevents the detection of a tsunami signal in either the target series or its spectrogram.

We present on Figure 9 a plot of the target and reference series for Track 073 following the Biak earthquake. It is apparent on this figure that the target series exhibits a high-frequency signal clearly identifiable in the space domain, in its southernmost part (between 275 and 900 km from the beginning of the trace), of which no counterpart can be found on the reference tracks, either in this region or farther North. It still appears in the space domain when the target series is subtracted from any reference series. The signal has two well-separated components, one centered 400 km into the series (at 0.9°N, 159.8°E), the other 800 km into the series (at 4.2°N, 161.0°E). Both are approximately 30 cm peak-to-peak. These locations are on the Ontong-Java Plateau, but not in its shallowest regions. The corresponding spectrogram (Plate 4a) has abundant energy in the band 0.004–0.02 km^{-1}. All cycles are noticeably noisy in the northern, noncausal, part of the track.

Tsunami synthetics were computed along Track 073 using the source model of the Biak earthquake derived by Y. Tanioka [*Tanioka et al.,* 1996; Y. Tanioka, personal communication, 1998], and are shown on Figure 10 (space domain) and Plate 4d (spectrogram). The synthetic amplitudes (maximum peak-to-peak 3.2 cm) are much smaller than the signal observed in the target series of Track 073. A multiplicative factor α of at least 20 would be necessary before the amplitude of the observed spectrogram could be matched by our synthetics (Plates 4g and 4h). We believe that such a large error in the geometry of source rupture is highly unlikely, especially since Tanioka's fault parameters were developed in part to successfully model the local tsunami around Biak and Yapen Islands. In addition, a robust characteristic of synthetics computed for a variety of slight alterations to Tanioka's source parameters is that their maximum amplitude takes place in the vicinity of the wavefront, not 1500 km behind it. Finally, the bathymetry in the area of the observed signal is shallow (2500 to 3500 m), but not sufficiently so as to create nonlinear amplifications in the wave field and render our finite-difference synthetics, computed under the shallow water approximations, inadequate. Thus, even though we cannot explain the origin of the signal observed at 0.9°N, 159.8°E, we must conclude against associat-

Plate 3. Spectrograms for the Chimbote tsunami along Track 180. This figure is comparable to Plate 1. Note in Plate 3a that the energy identified at 0.015 km^{-1} on Figure 7 is concentrated around a location 1600-2000 km into the series, and as such, noncausal with respect to the tsunami source. Also, the injection experiments (Plates 3d, 3e, 3f) show that the energy of the tsunami signal becomes detectable convincingly only on Plate 3e, suggesting $\alpha \approx 2.5$ as a threshold of detection.

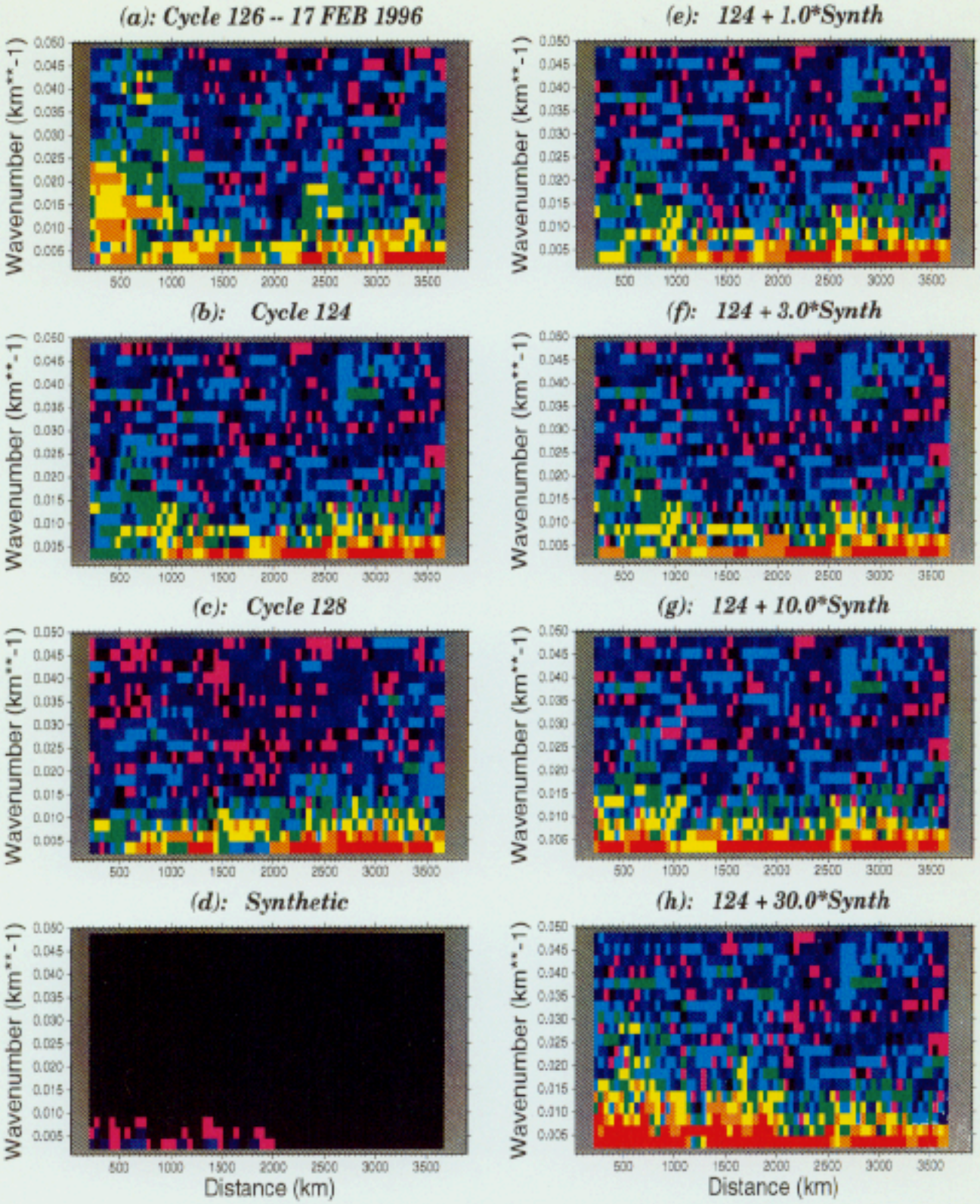
(a): Cycle 126 -- 17 FEB 1996
(b): Cycle 124
(c): Cycle 128
(d): Synthetic
(e): 124 + 1.0*Synth
(f): 124 + 3.0*Synth
(g): 124 + 10.0*Synth
(h): 124 + 30.0*Synth
Wavenumber (km**-1)
Distance (km)
6.00
4.00
3.80
3.60
3.40
3.20
3.00
2.75
2.50
15.00
Log-10 Spectral amplitude (m**2)

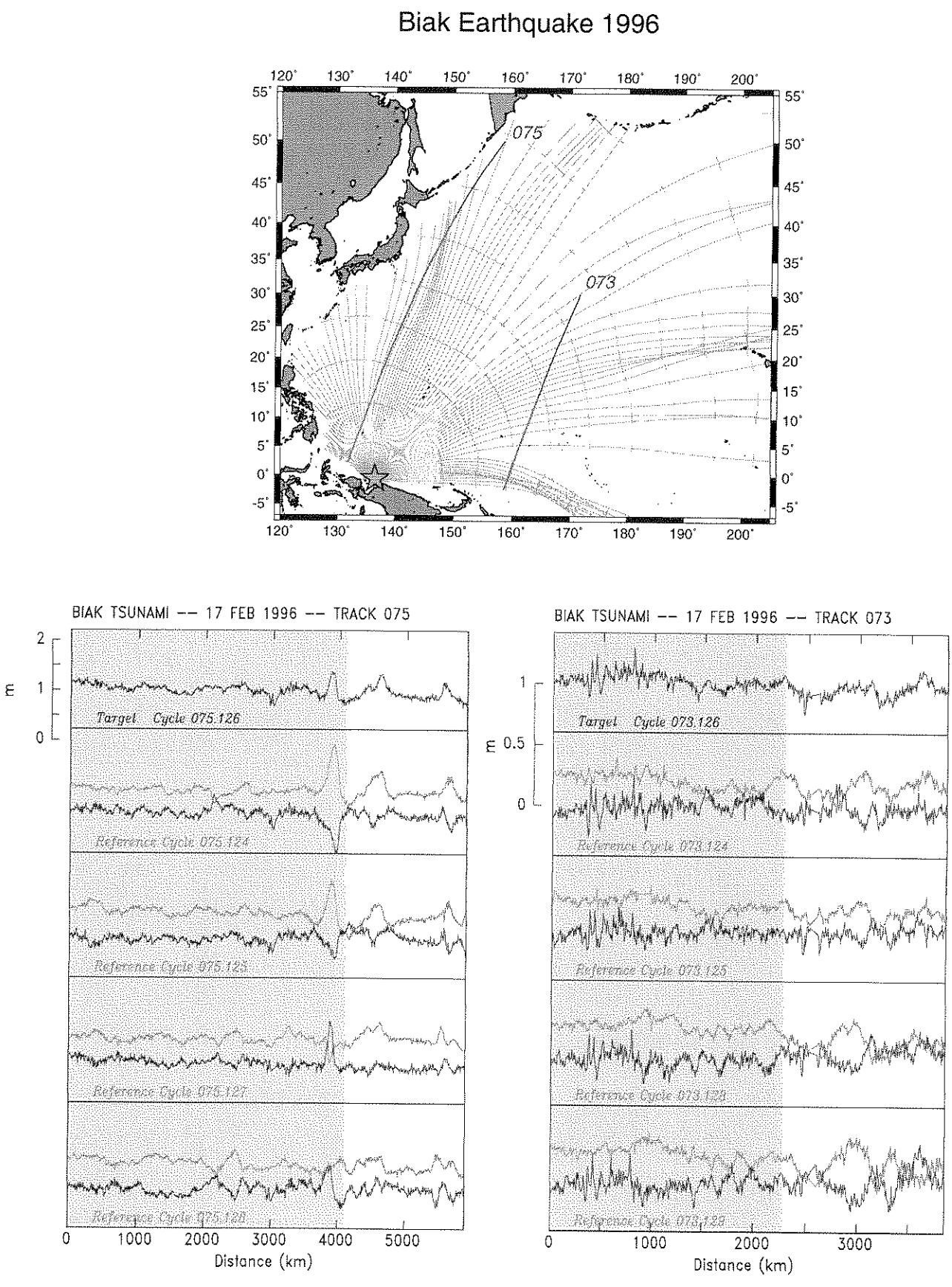

Figure 9. Case of the 1996 Biak tsunami. (top) Identification of the target tracks. The star indicates the epicenter. (bottom) as in Figure 2: (left) Track 075. Note that the signal is dominated by the signature of the Kuroshio current, approximately 4000 km into the series. (right) Track 073. Note the strong high-frequency signal toward the southern extremity of the target series, which, however, cannot be reconciled with acceptable synthetics.

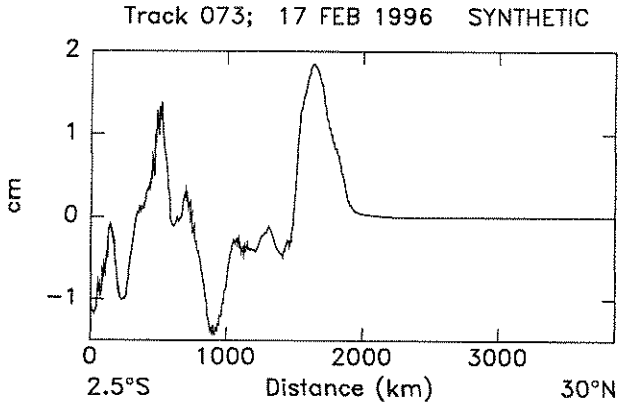

Figure 10. Synthetic maregram computed along Track 073 for Tanioka's fault model of the 1996 Biak earthquake.

ing it with the tsunami wave field. This is upheld by the fact that the signal detected has significant energy at relatively short wavelengths ($\Lambda_r = 50$ km), in a range where the synthetic's contribution is very weak, and by the low amplitude (2 cm peak-to-peak) of the tidal gauge signal at the nearby island of Pohnpei (M. Blackford, personal communication, 1998).

6.2. The Java Tsunami of June 2, 1994

Like the 1992 Nicaraguan event, this earthquake featured a slow rupture, presumably involving a sedimentary structure, and resulted in a significantly larger local tsunami than would have been expected from its seismic waves [*Tanioka and Satake,* 1996; *Newman and Okal,* 1998].

We identified Cycle 063 of T/P Track 077 as a target series, and Cycles 061, 062, 064 and 065 as references. While some energy is present at 0.010 km^{-1} in the target spectrograms, it does not rise above the background noise as expressed by Reference Cycles 061 and 065, and we conclude that the tsunami cannot be detected.

6.3. The Kuriles Tsunami of October 4, 1994

This very large earthquake ($M_0 = 3.0 \times 10^{28}$ dyn-cm) generated a significant tsunami which inflicted considerable damage on the Southern Kurile Islands [*Yeh et al.,* 1995]. However, because the earthquake was an intraplate event with substantial depth (its inverted centroid being at 68 km [*Dziewonski et al.* 1995]), it did not unleash a powerful Pacific-wide tsunami. We nevertheless sought to detect the tsunami signal in altimetry data sets, using Cycles 075 (target) and 073, 074, 076 and 077 (reference) of T/P Track 201. Unfortunately, as in the case of the Biak earthquake, the series are dominated by the signal of the Kuroshio current, and no signal convincingly attributable to the tsunami emerges from the spectrograms.

6.4. The Japan Sea Tsunami of July 12, 1993

This particular tsunami is totally contained in the Sea of Japan. The only target profile (Cycle 030 of T/P Track 127) has a total length over the sea of 600 km and is directed at a low angle to the wave front. The reference series (Cycles 029 and 033) show considerable noise at the low wavenumbers (0.005 to 0.01 km^{-1}) most prominent in the synthetic; the small extent of the profile does not allow an appropriate separation of long wavelengths along track, and we cannot detect this tsunami in the Sea of Japan.

7. Conclusion

The conclusions of this study are in a sense mixed. On the one hand, we have presented in the case of the 1992 Nicaraguan earthquake what constitutes to our knowledge the first direct detection and measurement of the deformation of the surface of the ocean in a tsunami wave field, on the high seas and unaffected by coastal effects. In particular, the similarity in dispersion found in the target series, the synthetics, and *González and Kulikov*'s [1993] Gulf of Alaska records, identifies the tsunami signal in the spectrogram of the target series. Modeling the spectral amplitudes of the detected signal requires a tsunami wave scaled by a factor $\alpha = 1.55$ with respect to the synthetic computed from *Piatanesi et al.*'s [1996] model, developed primarily to match regional run-up and inundation data along the Central American coast. We regard such a value of the ratio α as similar, for example, to the range of the typical scatter in moment values obtained when different investigators use different techniques to model the same large earthquake; in view of the uncertainties in source parameters mentioned above, we would certainly not regard its departure from unity as significantly degrading the detection. The peak-to-peak amplitude of the inferred tsunami wave field, 8 cm, corresponds to oscillations identifiable in the target series, but direct detection in the space domain may not be warranted.

In the case of the 1995 Chilean earthquake, the pulse of energy detected in the target series is most probably due to the tsunami wave field. However, the variability of the spectra of the various reference series lead to a scatter of a factor of 2 in the possible values of the ratio α, depending on which cycle is used as background noise. This prevents us from reaching a robust conclusion regarding the amplitude of the detected signal, and in order to stay on the safe side, we prefer to qualify this signal as a tentative detection.

On the other hand, we fail to detect several significant tsunamis, such as the 1996 Biak, the 1996 Chimbote, or the 1994 Java, tsunamis, the latter two being in many respects comparable to the 1992 Nicaraguan one. Indeed, among the seven events targeted in this study, the only confirmed detection is for the earthquake with the second-smallest seismic moment (Table 1). In this respect, our experience with Java, and with Tracks 523 (Nicaragua) and 230 (Chile), underscores the primary importance of directivity effects: in the latter two cases, the detection is possible (or probable) only on the later passage, i.e., at a greater epicentral distance, for which the wave would be expected to be of smaller amplitude, but along a path sampling tsunami rays that leave the source in the lobes of its directivity pattern. This means that for a detection to be achieved, not only must the satellite cross the wave front in an adequate space-time combination, but the portion of the wave field sampled must be favored in terms of directivity. Because the lobes of directivity functions become narrower as the dimension of the source grows [*Okal and Talandier,* 1991], this problem will not be simply compensated by growth in source size, and the influence of directivity is expected to remain crucial even for the largest tsunamis (as illustrated, for example, by the minimal amplitudes of the 1964 Alaskan tsunami in Hawaii and Polynesia). Directivity is probably the major effect preventing detection of the Biak tsunami in Micronesia, where ray tracing would suggest some positive focusing.

Our experience also indicates that a number of other factors contribute many sources of "noise" to the altimetric signal. Some of it, such as the geoid signature of the Nazca Ridge encountered on Track 523 for Nicaragua, is, of course, static and can be removed by subtracting reference series; some however, like the Kuroshio current, have a level of variability over the satellite's repeat period, which prevents this form of

processing, resulting in the masking of any potential signal of the Biak tsunami (and probably also of the Kuriles one), even though the geometry of Track 075 would have suggested a favorable directivity effect. Finally, there remain some unexplained transient signals; those occurring at noncausal space-time combinations, as in the case of Track 180 for the 1996 Peruvian tsunami, can be easily dismissed; on the other hand, the signal present in Track 073 of the Biak event had to be eliminated on account of our failure to match it from all reasonable models of the earthquake rupture.

As a final word, we want to stress that considerable insight into the characteristics of a tsunami wave on the high seas could and will certainly be gained from satellite observations of future large tsunamis. However, and given the handful of altimetry satellites presently operational, direct real-time detection of tsunami waves for the purpose of transoceanic tsunami warning is not presently feasible; our experience indicates that finding the satellite at the right place at the right time, i.e., under the right space-time combination of epicentral location, source directivity, and satellite ephemerides, remains the exception rather than the rule.

Acknowledgments. We are grateful to Philippe Gaspar and the Staff of Collecte Localisation Satellites, Toulouse, for providing the satellite altimetry data used in this work. Sandrine Guibourg helped with several synthetics in the early stages of the project. We thank Yuichiro Tanioka for providing his model of source ground motion for the Biak earthquake in advance of publication, Michael Blackford for a copy of the Biak tidal gauge record at Pohnpei, and Carolina Lithgow-Bertelloni for a personalized interlibrary loan. The paper benefited from careful reviews by John Vidale and Kenji Satake. This work was supported by CEA–DASE.

References

Ben-Menahem, A., Radiation of seismic surface waves from finite moving sources, *Bull. Seismol. Soc. Am., 51,* 401-435, 1961.

Ben-Menahem, A., and M. Rosenman, Amplitude patterns of tsunami waves from submarine earthquakes, *J. Geophys. Res., 77,* 3097-3128, 1972.

Birkett, C.M., The contribution of TOPEX/POSEIDON to the global monitoring of climatically sensitive lakes, *J. Geophys. Res., 100,* 25179-25204, 1995.

Braddock, R.D., Response of a conventional tide gauge to a tsunami, *Mar. Geod., 4,* 223-236, 1980.

Callahan, P.S., and W.H. Daffer, Search for earthquake effects in TOPEX/POSEIDON data (abstract), *Eos, Trans. AGU, 75, (44),* Fall Mtg. Supp., 357, 1994.

Cazenave, A., P. Bonnefond, K. Dominh, and P. Schaeffer, Caspian Sea level from TOPEX-POSEIDON altimetry: Level now falling, *Geophys. Res. Lett., 24,* 881-884, 1997.

Chelton, D.B., and M.G. Schlax, Global observation of oceanic Rossby waves, *Science, 272,* 234-238, 1996.

Dziewonski, A.M., A. Friedman, D. Giardini, and J.H. Woodhouse, Global seismicity of 1982: Centroid moment tensor solutions for 308 earthquakes, *Phys. Earth Planet. Inter., 33,* 76-90, 1983.

Dziewonski, A.M., G. Ekström, and M.P. Salganik, Centroid-moment tensor solutions for October-December 1994, *Phys. Earth Planet. Inter., 91,* 187-201, 1995.

Filloux, J.H., Tsunami recorded on the open ocean floor, *Geophys. Res. Lett., 9,* 25-28, 1982.

González, F.I., and Ye.A. Kulikov, Tsunami dispersion observed in the deep ocean, in: *Tsunamis in the World,* edited by S. Tinti, pp. 7-16, Kluwer Acad., Norwell, Mass., 1993.

González, F.I., C.L. Mader, M.C. Eble, and E.N. Bernard, The 1987–88 Alaskan Bight tsunamis: Deep ocean data and model comparisons, *Natural Hazards, 4,* 119-140, 1991.

Gründlingh, M.L., Tracking eddies in the Southeast Atlantic and Southwest Indian Oceans with TOPEX/POSEIDON, *J. Geophys. Res., 100,* 24977-24986, 1995.

Guibourg, S., P. Heinrich, and R. Roche, Numerical modeling of the 1995 Chilean tsunami; impact on French Polynesia, *Geophys. Res. Lett., 24,* 775-778, 1997.

Imamura, F., and N. Shuto, Analysis of OBS data and numerical simulation for the 1990 Mariana earthquake tsunami, in: *Tsunamis in the World,* edited by S. Tinti, pp. 95-106, Kluwer Acad., Norwell, Mass., 1993.

Kanamori, H., Mechanism of tsunami earthquakes, *Phys. Earth Planet. Inter., 6,* 346-359, 1972.

Kanamori, H., and M. Kikuchi, The 1992 Nicaragua earthquake: a slow tsunami earthquake associated with subducted sediments, *Nature, 361,* 714-716, 1993.

Kikuchi, M., and H. Kanamori, Source characteristics of the 1992 Nicaragua tsunami earthquake inferred from teleseismic body waves, *Pure Appl. Geophys., 144,* 441-453, 1995.

Landisman, M., A. Dziewonski, and Y. Satô, Recent improvements in the analysis of surface wave observations, *Geophys. J. Roy. astr. Soc., 17,* 369-403, 1969.

Mader, C.L., *Numerical Modeling of Water Waves,* Univ. of Calif. Press, Berkeley, 1988.

Newman, A.V., and E. A. Okal, Source slowness of the February 21, 1996 Chimbote earthquake studied from teleseismic energy estimates (abstract), *Eos, Trans. AGU, 77, (17),* Spring Mtg. Supp., S184, 1996.

Newman, A.V., and E.A. Okal, Teleseismic estimates of radiated seismic energy: The E/M_0 discriminant for tsunami earthquakes, *J. Geophys. Res., 103,* 26885–26898, 1998.

Okada, M., Ocean-bottom pressure gauge for tsunami warning system in Japan, in: *Proceedings of the 2nd UJNR Tsunami Workshop,* pp. 219–227, NOAA, Boulder, Colo., 1991.

Okada, Y., Surface deformation due to shear and tensile faults in a half-space, *Bull. Seismol. Soc. Am., 75,* 1135-1154, 1985.

Okal, E.A., Mode-wave equivalence and other asymptotic problems in tsunami theory, *Phys. Earth Planet. Inter., 30,* 1-11, 1982.

Okal, E.A., Seismic parameters controlling far-field tsunami amplitudes: A review, *Natural Hazards, 1,* 67-96, 1988.

Okal, E.A., Seismotectonic setting of the February 17, 1996 Biak, Indonesia earthquake (abstract), *Eos, Trans. AGU, 77, (17),* Spring Mtg. Suppl., S184, 1996.

Okal, E.A., and J. Talandier, Single-station estimates of the seismic moment of the 1960 Chilean and 1964 Alaskan earthquakes, using the mantle magnitude M_m, *Pure Appl. Geophys., 136,* 103-126, 1991.

Piatanesi, A., S. Tinti, and I. Gavagni, The slip distribution of the 1992 Nicaragua earthquake from tsunami run-up data, *Geophys. Res. Lett., 23,* 37-40, 1996.

Ruegg, J.-C., et al., The $M_w = 8.1$ Antofagasta (North Chile) earthquake of July 30, 1995: First results from teleseismic and geodetic data, *Geophys. Res. Lett., 23,* 917-920, 1996.

Schindelé, F., D. Reymond, E. Gaucher, and E.A. Okal, Analysis and automatic processing in near-field of the eight 1992-1994 tsunamigenic earthquakes: Improvements in real-time tsunami warning, *Pure Appl. Geophys., 144,* 381–408, 1995.

Tanioka, Y., and K. Satake, Tsunami displacement by horizontal displacement of ocean bottom, *Geophys. Res. Lett., 23,* 861-864, 1996.

Tanioka, Y., L.J. Ruff, and K. Satake, The recent large tsunamigenic earthquakes (abstract), *Eos, Trans. AGU, 77, (17),* Spring Mtg. Suppl., S184, 1996.

Teague, W.J., Z.R. Hallock, G.A. Jacobs, and J.L. Mitchell, Kuroshio sea surface fluctuations observed simultaneously with inverted echo sounders and TOPEX/POSEIDON, *J. Geophys. Res., 100,* 24987-24994, 1995.

Ward, S.N., Relationships of tsunami generation and an earthquake source, *J. Phys. Earth, 28,* 441-474, 1980.

Woods, M.T., and E.A. Okal, Effect of variable bathymetry on the amplitude of teleseismic tsunamis: a ray-tracing experiment, *Geophys. Res. Lett., 14,* 765-768, 1987.

Wunsch, C., and D. Stammer, The global frequency-wavenumber spectrum of oceanic variability estimated from TOPEX/POSEIDON altimetric measurements, *J. Geophys. Res., 100,* 24895–24910, 1995.

Yeh, H., V. Titov, V. Gusiakov, E. Pelinovsky, V. Khramushin, and V. Kaistrenko, The 1994 Shikotan earthquake tsunamis, *Pure Appl. Geophys., 144,* 855-874, 1995.

P. Heinrich and A. Piatanesi, Département Analyse et Surveillance de l'Environnement, Commissariat à l'Energie Atomique, B.P. 12, F–91680 Bruyères-le-Châtel, France.

E.A. Okal, Department of Geological Sciences, Northwestern University, Evanston, IL 60208, USA.

(Received June 9, 1998; revised August 27, 1998;
accepted September 19, 1998.)